Role of ELOVL4 and very long-chain polyunsaturated fatty acids in mouse models of Stargardt type 3 retinal degeneration

Peter Barabas[a,1], Aihua Liu[a], Wei Xing[a], Ching-Kang Chen[b], Zongzhong Tong[a], Carl B. Watt[a], Bryan W. Jones[a], Paul S. Bernstein[a], and David Križaj[a,c,1]

Departments of [a]Ophthalmology and Visual Sciences and [c]Physiology, Moran Eye Institute, University of Utah, Salt Lake City, UT 84132; and [b]Department of Biochemistry and Molecular Biology, Virginia Commonwealth University, Richmond, VA 23298

Edited by Jeremy Nathans, Johns Hopkins University, Baltimore, MD, and approved February 15, 2013 (received for review August 24, 2012)

Stargardt type 3 (STGD3) disease is a juvenile macular dystrophy caused by mutations in the *ELOVL4* (*Elongation of very long chain fatty acids 4*) gene. Its protein product, ELOVL4, is an elongase required for the biosynthesis of very long-chain polyunsaturated fatty acids (VLC-PUFAs). It is unclear whether photoreceptor degeneration in STGD3 is caused by loss of VLC-PUFAs or by mutated ELOVL4 protein trafficking/aggregation. We therefore generated conditional knockout (cKO) mice with *Elovl4* ablated in rods or cones and compared their phenotypes to transgenic (TG) animals that express the human STGD3-causing $ELOVL4^{STGD3}$ allele. Gas chromatography–mass spectrometry was used to assess C_{30}–C_{34} VLC-PUFA and *N*-retinylidene-*N*-retinylethanolamine content; electroretinography was used to measure phototransduction and outer retinal function; electron microscopy was used for retinal ultrastructure; and the optomotor tracking response was used to test scotopic and photopic visual performance. *Elovl4* transcription and biosynthesis of C_{30}–C_{34} VLC-PUFAs in rod cKO and TG retinas were reduced up to 98%, whereas the content of docosahexaenoic acid was diminished in TG, but not rod cKO, retinas. Despite the near-total loss of the retinal VLC-PUFA content, rod and cone cKO animals exhibited no electrophysiological or behavioral deficits, whereas the typical rod–cone dystrophic pattern was observed in TG animals. Our data suggest that photoreceptor-specific VLC-PUFA depletion is not sufficient to induce the STGD3 phenotype, because depletion alone had little effect on photoreceptor survival, phototransduction, synaptic transmission, and visual behavior.

Proper development and functioning of the mammalian nervous system depends on adequate levels of C_{14}–C_{22} long-chain polyunsaturated fatty acids (LC-PUFAs), such as omega-6 (n6) (i.e., arachidonic acid, C_{20}:4n6) and omega-3 (n3) [i.e., eicosapentaenoic acid (EPA; C_{20}:5n3) and docosahexaenoic acid (DHA; C_{22}:6n3)] species, and "very long-chain" (VLC) (C_{24}–C_{36}) PUFAs. In contrast to abundant and ubiquitous expression of LC-PUFAs, VLC-PUFA biosynthesis is restricted to select types of cells (spermatocytes, fibroblasts, keratinocytes, and photoreceptors) where they may be necessary to stabilize highly curved cellular membranes (1–3). Both LC- and VLC-PUFAs are generated through an elongation process in the endoplasmic reticulum (ER) where resident Elongation of very long-chain fatty acids 2 (ELOVL2) and ELOVL4 elongases add two-carbon units to the acyl backbone (2, 4).

The discovery that ELOVL4 mutations can compromise vision in humans and mice has provided an important clue that VLC-PUFAs may be required for normal neuronal function. Three sets of mutations (789delT plus 794delT, 790–794delAACTT, and Y270X) cause the autosomal dominant Stargardt-like macular dystrophy type 3 (STGD3; Online Mendelian Inheritance in Man 600110) that is characterized by progressive loss of central vision starting during adolescence (3, 5–7). The severity of human STGD3 is inversely associated with dietary intake of VLC-PUFA precursors (8). It is currently unclear whether and to what degree photoreceptor loss observed in age-related macular degeneration (AMD) patients (9), STGD3 patients (10), and transgenic (TG) mouse STGD3 models (11–13) are primarily caused by loss of VLC-PUFAs (4, 8, 14), from secondary dominant negative consequences of protein aggregation, ER stress, and induction of the unfolded protein response (UPR) (15–18) or from reduced biosynthesis of DHA (6).

Global homozygous *Elovl4* knockout and knock-in of the human mutation into the mouse *Elovl4* gene cause death of newborn mice due to loss of skin VLC acyl-ceramides, which are required to maintain the water barrier function (19–21). To circumvent postnatal lethality, we generated mouse strains in which *Elovl4* was selectively eliminated from rods [rod conditional knockouts (cKOs)] or cones (cone cKOs) and compared their phenotypes to TG mice that express the human STGD3-causing *ELOVL4* allele ($ELOVL4^{STGD3}$). Our data demonstrate that near-total depletion of VLC-PUFAs does not induce STGD3-like phenotype in the adult mouse retina, suggesting that a normal VLC-PUFA level is not required for rod and cone function or survival.

Results

Conditional Elimination of *Elovl4* Is Not Associated with Loss of Photoreceptor Gene Markers or Outer Retina Morphology Changes. The parental $Elovl4^{flox/flox}$ (floxed) strain was created by introducing two *loxP* (locus of crossing-over in phage P1) sites, upstream of exon 2 and downstream from exon 3, respectively. *Elovl4* was ablated from rods or cones by breeding floxed animals with rod-specific *opsin–cre* (rod cKO1), *opsin–iCre75* (rod cKO2), and cone-specific human red-green pigment (*HRGP*)–*cre* mice (cone cKO). Loss of the gene was confirmed with RT-PCR (Fig. 1*A*), and proper targeting of the recombinase was assessed by double-labeling retinas with ELOVL4 and Cre-specific antibodies (Fig. 1 *B* and *C*). The *cre* drivers (22, 23) used to generate two distinct rod cKO strains produced different degrees of *Elovl4* knockdown. Eliciting ~89% decrease in *Elovl4* mRNA (11.4 ± 2.7% of congenic control), the knockdown was more efficient in *opsin–iCre75* mice (rod cKO2) compared with *opsin–Cre* retinas (rod cKO1) (39.2 ± 8.1% of controls; Fig. 1*A*). Accordingly, columns of Cre-negative ELOVL4-positive rods were observed within the cKO1 outer nuclear layer (ONL), indicating incomplete ablation of *Elovl4* (Fig. 1*C*). Such Cre-negative columns were never detected in *opsin–iCre75* retinas in which the overwhelming majority of rod perikarya were immunopositive for Cre (Fig. 1 *D* and *E*). Cones in rod cKO retinas were not labeled by the Cre antibody (Fig. 1*F*). As shown (24), Cre expression was

Author contributions: P.B., A.L., P.S.B., and D.K. designed research; P.B., A.L., W.X., C.B.W., B.W.J., and D.K. performed research; C.-K.C. and Z.T. contributed new reagents/analytic tools; P.B., A.L., and P.S.B. analyzed data; and P.B. and D.K. wrote the paper.

The authors declare no conflict of interest.

This article is a PNAS Direct Submission.

[1]To whom correspondence may be addressed. E-mail: peter.barabas@utah.edu or david.krizaj@hsc.utah.edu.

This article contains supporting information online at www.pnas.org/lookup/suppl/doi:10.1073/pnas.1214707110/-/DCSupplemental.

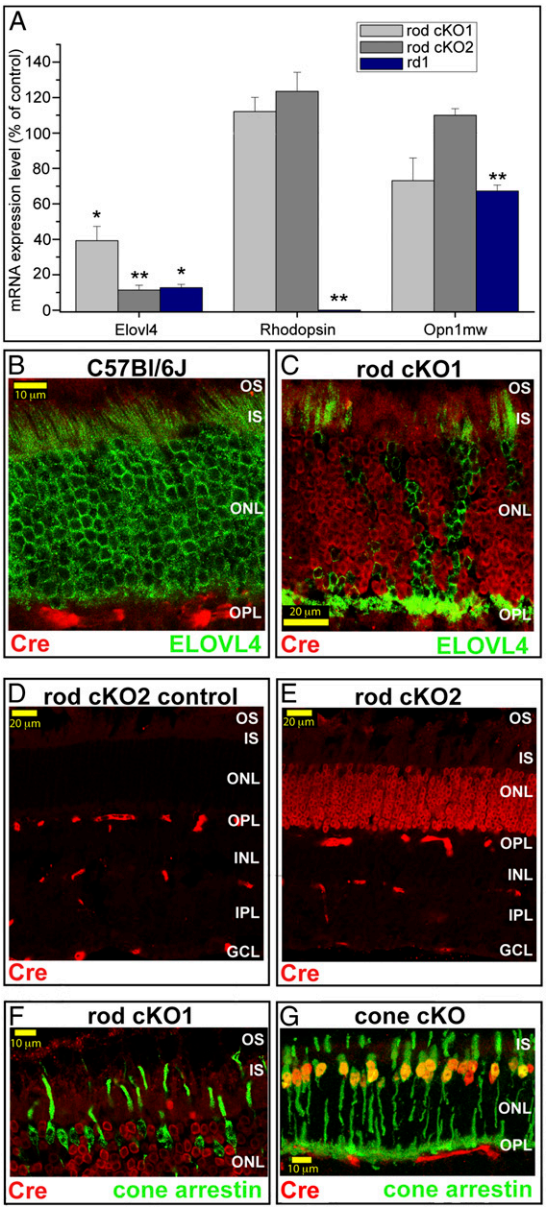

Fig. 1. (*A*) RT-PCR for *Elovl4*, *Rho*, and *Opn1mw* confirmed the efficiency of ELOVL4 knockdown in rod cKO2 and in 3-mo-old *rd1* rodless retinas. cKO, but not *rd1*, retinas maintained normal levels of rod and cone markers (expression levels are expressed as percentage of age-matched congenic *cre*$^{-}$ control values for the cKO strains; age-matched C57BL/6J retinas represented *rd1* controls). (*B*) ELOVL4 immunoreactivity in C57BL/6J photoreceptors. (*C*) Rod cKO1 retina. *Cre* and *Elovl4* expression in the ONL is mutually exclusive. Most rods express Cre (Alexa 594 nm) except for columnar patches of cells that express ELOVL4 (Alexa 488 nm). (*D* and *E*) Cre-immunofluorescence in rod cKO2 *cre*$^{-}$ and cre^{+} retinas. (*F*) No cones (labeled with cone arrestin; Alexa 488) were colabeled for cre (Alexa 594), present only in rods. (*G*) Every cone (cone arrestin; Alexa 488) in the cone cKO model is immunopositive for cre (Alexa 594) (projection image of an 8-μm Z-stack). GCL, ganglion cell layer; IPL, inner plexiform layer; INL, inner nuclear layer; OPL, outer plexiform layer; ONL, outer nuclear layer; IS, inner segments; OS, outer segments. *$P < 0.05$; **$P < 0.01$.

observed in every cone arrestin-positive *HRGP–cre*$^{+}$ cell in cone cKO retinas (Fig. 1*G*).

To determine whether conditional ablation affected expression of typical photoreceptor cell markers, we analyzed the cKO retinas for rod (rhodopsin; *Rho*) and cone (cone middle wavelength opsin; *Opn1mw*) mRNA. As shown in Fig. 1*A*, *Rho* and *Opn1mw* mRNA levels in 5- to 7-mo-old rod cKO retinas exhibited no decreases compared with transcript levels measured in age-matched floxed *cre*$^{-}$ controls (*Rho*, rod cKO1: $P = 0.2527$, rod cKO2: $P = 0.3294$; *Opn1mw,* rod cKO1: $P = 0.1343$, rod cKO2: $P = 0.7992$). This result indicates that, in contrast to the observations in TG retinas expressing ELOVL4^{STGD3} (11, 12), conditional elimination of the gene from rods does not result in rod loss. The data also suggest that cKO rods do not undergo the global reduction of transcription that is characteristic for UPR (25).

Consistent with the RT-PCR data, histological and electron microscopic analysis of 8.6-mo-old rod cKO1 retinas (Fig. 2) revealed no marked abnormalities in the number of photoreceptor cell rows (Fig. 2*E*; 8.5 ± 0.8 rows, $n = 4$ cKOs vs. 8.3 ± 0.6 rows in $n = 4$ controls; $P = 0.8778$) or ONL thickness (30.6 ± 3.5 μm vs. 28.8 ± 2.5 μm in controls; $P = 0.6912$). The ultrastructure of rod outer segments from rod cKO1 mice showed no abnormalities (Fig. 2 *A* and *C*). Although lipid droplets were occasionally detected in rod cKO1 retinal pigmented epithelium (RPE) cells (Fig. 2*D*, white arrows), they were also observed in control retinas and never exhibited features characteristic of *N*-retinylidene-*N*-retinylethanolamine (A2E)/lipofuscin accumulation. Similarly, we found no structural abnormalities in plastic sections and EM photomicrographs of rod cKO2 retinas (Fig. S1 and Fig. 2 *A* and *C*).

To control for the photoreceptor-specific expression of *Elovl4*, we also examined its expression in 3-mo-old *rd1* (*phosphodiesterase 6b*^{rd1}) mouse retinas manifesting near-total loss of rods (26). Consistent with the predominant localization of *Elovl4* gene expression to photoreceptors, its transcripts in adult *rd1* retinas were reduced to 12.7 ± 1.9% of control, age-matched C57BL/6J levels ($P = 0.0139$). The decreases in *Rho* (2.4 ± 2.4% of control; $P = 0.0035$), and *Opn1mw* (20.4 ± 8.6%, $P = 0.0090$) mRNAs in *rd1* retinas were in marked contrast to the normal levels of visual pigment mRNAs and intact ONL structure observed in cKO retinas (Figs. 1*A* and 2). The lack of the cKO phenotype was surprising, given that retinas from the STGD3 TG mouse model (the "TG" strain) exhibit substantial photoreceptor degeneration by 3–6 mo (11).

VLC-PUFA Content Decreases in *Elovl4* cKO and TG Retinas. GC-MS measurements in pairs of retinas from individual cKO and TG (*ELOVL4*^{STGD3}) animals were performed to determine the relationship between *Elovl4* knockdown and retinal C_{30}–C_{34} VLC-PUFA content. Statistically significant decreases in VLC-PUFA content were observed for rod cKO1 (Fig. S2*A*), cKO2 (Fig. 3*A* and Fig. S2*A*; $P = 0.0048$), and TG (32.2 ± 2.3% of control at 1 mo; Fig. 3*C*; $P < 0.0001$), but not cone cKO samples (161.4 ± 16.5% of control; Fig. 3*B*; $P = 0.0895$). The extent of the decrease differed between the strains with the rod cKO1 strain showing the smallest decrease (42.0 ± 7.3% of control; $P = 0.0053$; Fig. S2*A*). In 5-mo-old rod cKO2 retinas, the total VLC-PUFA content decreased by 97.7 ± 0.2% ($P = 0.0023$), whereas in 1-, 2-, and 4-mo-old TG retinas VLC-PUFA levels were reduced by 67.8 ± 2.3%, 93.3 ± 1.0%, and 97.6 ± 0.1%, respectively. VLC-PUFAs were undetectable in 7-mo-old TG retinas (Fig. 3 *C* and *D*). Targeted elimination of *Elovl4* from rods and introduction of the *ELOVL4*^{STGD3} transgene are equally efficacious in suppressing the biosynthesis of VLC-PUFAs.

An n3/n6 imbalance has been associated with retinal diseases (9, 27). We therefore assessed the n3/n6 ratio for cKO and TG retinas by comparing the ratio of C_{30}:5n3, C_{32}:6n3, C_{32}:5n3, C_{34}:6n3, and C_{34}:5n3 to C_{32}:4n6 fatty acids (FAs). A significant decrease in the ratio to 2.58 ± 1.03% of control levels was observed in rod cKO2 retinas ($P = 0.0006$; Fig. 3*E*). There was no detectable change in the n3/n6 ratio for cone cKO ($P = 0.9365$) mice (Fig. 3*E*). Changes in the n3/n6 ratio for TG retinas (40.1 ± 8.6%, 81.3 ± 4.8%, and 72.6 ± 0.9% reduction in 1-, 2-, and 4-mo-old retinas, respectively) paralleled the loss of *Elovl4* function and the overall reduction of VLC-PUFA content (Fig. 3*F*).

The DHA content in rod cKO1 (24.0 ± 1.2 peak area percentage, age: 5 mo; $P = 0.9141$) and rod cKO2 (27.1 ± 0.8% peak area,

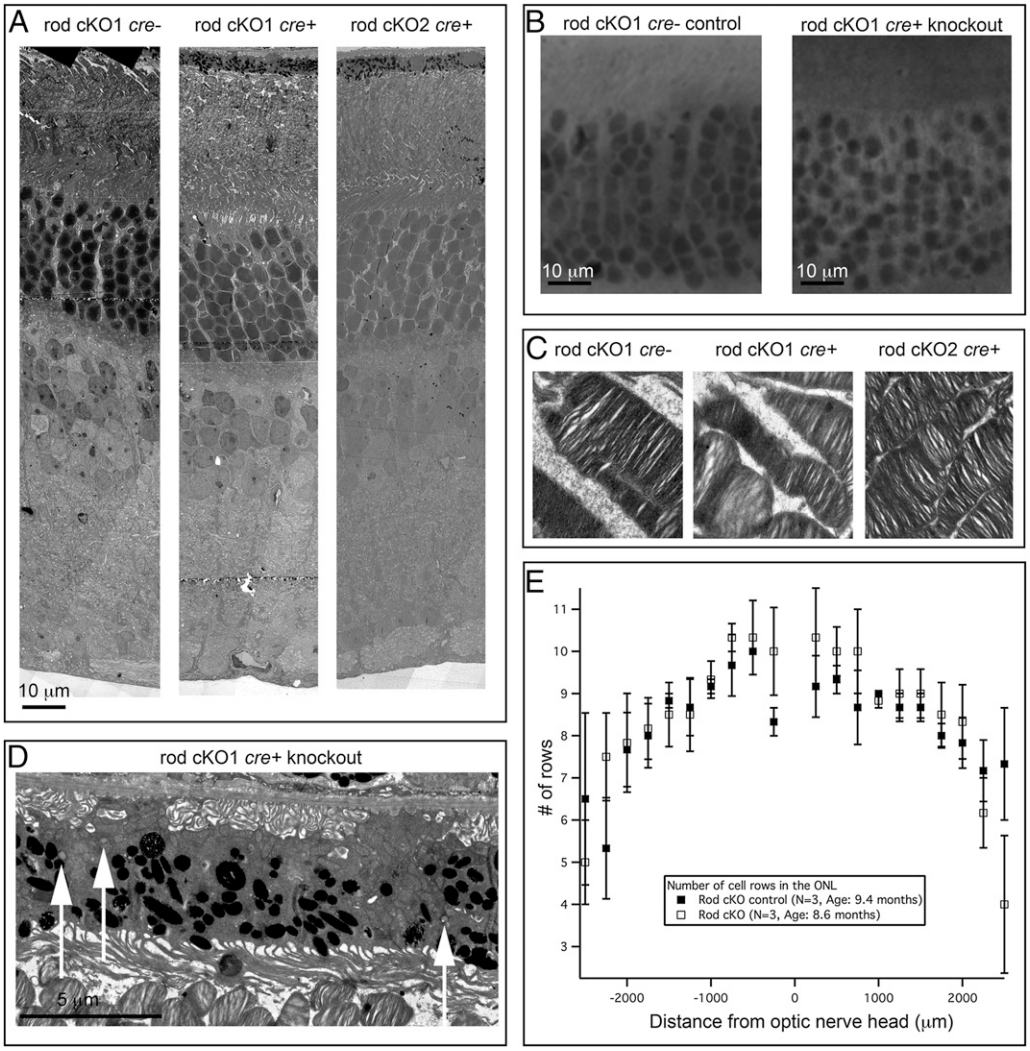

Fig. 2. (*A* and *B*) The 8.6-mo-old rod cKO1 retinas and 9-mo-old rod cKO2 showed no structural deficits, as determined by electron microscopic (*A*) and standard histological (*B*) evaluation of toluidine blue-stained sections. (*C*) Rod outer segment ultrastructure was not affected in either cKO1 or cKO2 strains. (*D*) Although putative lipid droplets were found (white arrows) in cKO1 RPE, these did not show hallmarks of lipofuscin accumulation. (*E*) Analysis of number of photoreceptor cell rows did not reveal a significant difference between rod cKO1 knockouts and *cre*$^{-}$ controls.

age: 5 mo; $P = 0.0722$) retinas was not different from congenic controls (Fig. S2*B*), whereas slightly below-normal DHA levels were detected in 1-mo-old TG retinas (20.6 ± 0.4% peak area or 92.3 ± 1.8% of control; $P = 0.0256$). EPA levels were not affected in any of the cKO strains (Fig. S2*C*; rod cKO1: 96.0 ± 13.9% of control, $P = 0.8061$; rod cKO2 81.6 ± 8.3% of control, $P = 0.0955$; cone cKO: 92.8 ± 5.9% of control, $P = 0.3421$). Similarly, total A2E levels in rod cKO2 mouse eyes were not different (23.3 ± 4.2 pmoles per eye, $n = 5$, age: 9.6 mo; *t* test, $P = 0.8546$) from controls (26.3 ± 3.6 pmoles per eye, $n = 5$, age: 8.9 mo).

Together, these data show that conditional elimination of photoreceptor *Elovl4* results in substantial loss of retinal VLC-PUFAs but has no effect on retinal A2E or DHA content. Decreased DHA levels in TG retinas may be attributed to the progressive loss of rods.

Visual Behavior and Electroretinography Are Unaffected in cKO Mice. Having ascertained that ablation of *Elovl4* and the presence of ELOVL4^{STGD3} protein reduce retinal VLC-PUFA content, we investigated whether VLC-PUFAs are required for visual function. Light responses and synaptic output of rod and cone photoreceptors were determined by measuring scotopic and photopic flash electroretinography (ERG) field potentials (28, 29). Surprisingly, no significant differences in the amplitude of scotopic a- and b-waves were detected in either rod cKO1, rod cKO2, or cone cKO mice compared with their respective *cre*$^{-}$ controls up to 6.5 mo of age (Fig. 4*G*). Likewise, cKO b-wave responses recorded under photopic conditions were statistically indistinguishable from b-waves measured in control eyes (Fig. 4*G*; $P = 0.4232$ for cone cKOs; $P = 0.5276$ for rod cKO2s). No difference between scotopic or photopic a-wave amplitudes was observed for the three cKO lines at any of the tested intensities. To assess the visual performance of VLC-PUFA–depleted mice, we used the optomotor tracking test (30–32). The spatial frequency still eliciting an optomotor reflex in 3- to 6-mo-old rod cKO animals tested under scotopic and photopic conditions was similar to controls. Likewise, no deterioration of photopic threshold level was observed in the cone cKO strain up to 10 mo (Fig. 4*C*; $n = 15$ and 16 for control and cKO mice; $P = 0.2513$). These data demonstrate that up to 98% decrease in retinal VLC-PUFA levels does not affect outer retinal function or visual performance within the studied age window.

Functional Deficits in the TG Strain Are Consistent with Rod–Cone Dystrophy. Although showing decreases in retinal VLC-PUFA content that were comparable with rod cKO retinas, TG mice exhibited a progressive decline of ERG parameters (Fig. 4 *D–F* and *H*) and visual performance (Fig. 4 *C* and *H*). The fall-off in the amplitude of scotopic a- and b-waves in TG retinas mirrored the decreases in the n3/n6 ratio, retinal DHA, and VLC-PUFA content (Fig. 4*H*). Scotopic b-wave amplitudes elicited by flashes of increasing intensity declined at all tested flash intensities starting at 1.4 mo (Fig. 4*E*), whereas photopic b-waves did not decrease until after 4 mo (Fig. 4*F*).

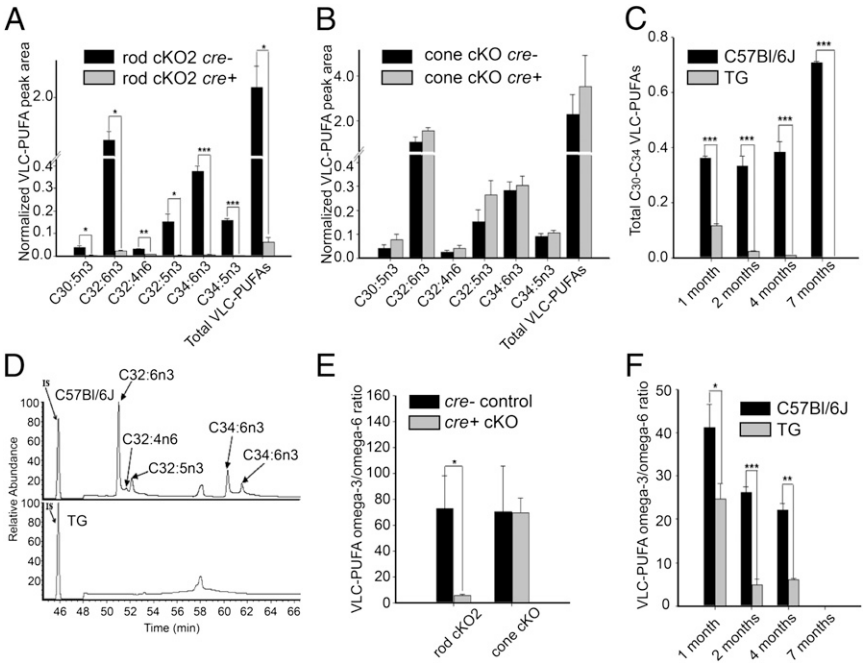

Fig. 3. (*A*) VLC-PUFA content in 5-mo-old rod cKO2 mouse retinas is significantly decreased compared with the control rod cKO2 *cre*$^{-}$ mouse retinas. (*B*) VLC-PUFA content in 5-mo-old cone cKO mouse retinas is unchanged compared with their congenic control. (*C*) The VLC-PUFA content of TG mouse retinas shows progressive loss from 1 to 4 mo; VLC-PUFAs are not measurable at 7 mo. (*D*) Representative GC-MS chromatograms of VLC-PUFAs. *Upper* and *Lower* represent VLC-PUFA (C_{32} and C_{34} groups) chromatograms for 7-mo-old C57BL/6J and TG mouse retinas, respectively. IS, internal standard (hentriacontanoic acid). (*E*) The n3/n6 ratio of VLC-PUFAs in 5-mo-old rod cKO2 mouse retinas is significantly decreased compared with control mice. There is no significant difference of n3/n6 ratios between cone cKO and *cre*$^{-}$ control mouse retinas. (*F*) The VLC-PUFA n3/n6 ratio in TG mouse retinas is significantly decreased compared with WT controls. $*P < 0.05$; $**P < 0.01$; $***P < 0.001$.

Scotopic optomotor behavior in TG mice exhibited an intriguing time course in which a mild deficit in optokinetic tracking before 2.5 mo (25.0 ± 1.5% decrease; $P < 0.0001$) was associated with a 77.7 ± 2.1% decline in the scotopic ERG a-wave, whereas a further 5% drop in scotopic a-wave (to 83.3 ± 2.1%) at 4 mo was linked to a catastrophic loss of optomotor responsiveness (Fig. 4*H*, open black squares). It is noteworthy that, at this age (4 mo), VLC-PUFA levels in TG retinas declined to <5% of controls (Fig. 3*C*). Scotopic a- and b-wave amplitudes in 4-mo-old mice remained at ∼17% and ∼33% of control ERG signals, respectively. At 7 mo, when retinal VLC-PUFA levels declined below detectability, DHA levels decreased to ∼51.9 ± 2.3% of control, scotopic ERG a-waves were depressed to <5%, and TG animals exhibited no scotopic optomotor behavior. The mismatched time course of scotopic b-wave responses and optomotor visual performance suggests that this type of visual behavior in mice can be evoked despite marked photoreceptor loss as long as a critical level of functioning photoreceptor input is maintained.

In contrast to the progressive loss of scotopic light-evoked responses and visual behavior, photopic behavioral performance in the TG strain remained at >95% of the normal response up to ∼3 mo (98.3 ± 2.0% of control; $P = 0.7773$ at 3.4 mo). A gradual decline in optomotor function was observed between 4 and 5.5 mo and was followed by total loss of function at >7.6 mo (Fig. 4*C*). The photopic b-wave amplitude in TG mice was largely unaffected or increased in the first 4 mo but dropped precipitously by 6.6 mo (to 8.2 ± 7.3 μV vs. 125.1 ± 13.3 μV in 6.3-mo-old control mice; $P = 0.0205$) (Fig. 4*F*). Thus, photoreceptor function in the STGD3 mouse follows a typical rod–cone dystrophic trajectory.

In vitro studies suggested that ER stress might represent a potential pathological signal in cells expressing mutant ELOVL4 (15–18). To test this mechanism, we measured mRNA levels of key modulators associated with the UPR (Fig. S3). Serine/threonine-protein kinase/endoribonuclease (*Ire1*) mRNA levels in TG retinas were at 106.1 ± 20.7% ($n = 12$; $P = 0.8012$), CCAAT/enhancer-binding protein homologous protein (*Chop*) at 108.7 ± 8.4% ($n = 4$; $P = 0.7286$), and binding immunoglobulin protein/glucose-regulated protein 78 (*Bip*/*Grp78*) at 125.9 ± 27.8% ($n = 12$; $P = 0.4380$) of controls. Likewise, no statistically significant differences were observed for activating transcription factor 6 (*Atf6*) (142.9 ± 10.1% of control; $n = 4$; $P = 0.4424$) and PKR-like ER kinase (*Perk*) (104.3 ± 6.0%; $n = 4$; $P = 0.8913$). In stark contrast to the absence of UPR, glial fibrillary acidic protein (*Gfap*) mRNA levels were markedly up-regulated (704.0 ± 70.8%; $n = 4$; $P = 0.0017$), paralleled with increased GFAP protein in radial glia (Fig. S4).

Discussion

Here we report data that clarify the role of ELOVL4-derived FAs in retinal dystrophy and visual function. VLC-PUFAs are generally rare FAs that comprise a large proportion (∼12%) of newly formed retinal lipids (33). Consistent with their importance for human vision, clinical studies showed reduced VLC-PUFA levels in AMD donor eyes (9) and an inverse association between the severity of STGD3 and dietary intake of VLC-PUFA precursors (8). A key role for VLC-PUFAs in the regulation of phototransduction and/or photoreceptor survival was also suggested by the observations of anatomical and functional deficits in TG mouse models deficient in C_{28}–C_{36} acyl phosphatidylcholines (4, 12, 14, 21). By demonstrating normal visual signaling and behavior in cKOs, our results challenge the hypothesis that VLC-PUFAs are required for murine photoreceptor development, survival, or function.

Our data confirm the central role of ELOVL4 in biosynthesis of photoreceptor VLC-PUFAs (4, 34). Conditional elimination of the elongase from rods or introduction of the human *STGD3* mutant allele resulted in near-total loss of retinal VLC-PUFAs. Surprisingly, such a dramatic decrease produced no discernable anatomical, electrophysiological, or visual behavioral abnormalities in cKO animals, suggesting that neither ELOVL4 nor its FA products are necessary for photoreceptor function. Although we cannot exclude the possibility that the fraction of photoreceptor cells with unablated *Elovl4* (e.g., cones in rod cKOs) rescued KO rods through the photoreceptor–RPE LC-PUFA shuttle mechanism (35), we consider this route insufficient given the small (3–5%) fraction of cones (36). Our results differ from a recent study that showed ∼25–45% decreases in the amplitudes of rod and cone-driven ERG b-waves in retinas with conditionally ablated *Elovl4* gene (34). We note that for adequate comparison of cKO results it is essential to use age-matched *cre*$^{-}$ *flox*$^{+}$/*flox*$^{+}$ control mice rather than generic wild-type (WT) strains. Another critical question pertains to the efficacy of *Elovl4* knockdown.

We find that the *opsin–cre* driver used in both studies (the rod cKO1 strain in our study; rod cKO in ref. 34) is only expressed in a subset of rods. *Elovl4* targeting in *opsin–Cre Elovl4*$^{fl+/fl+}$ mice produced an incomplete knockdown reducing total retinal

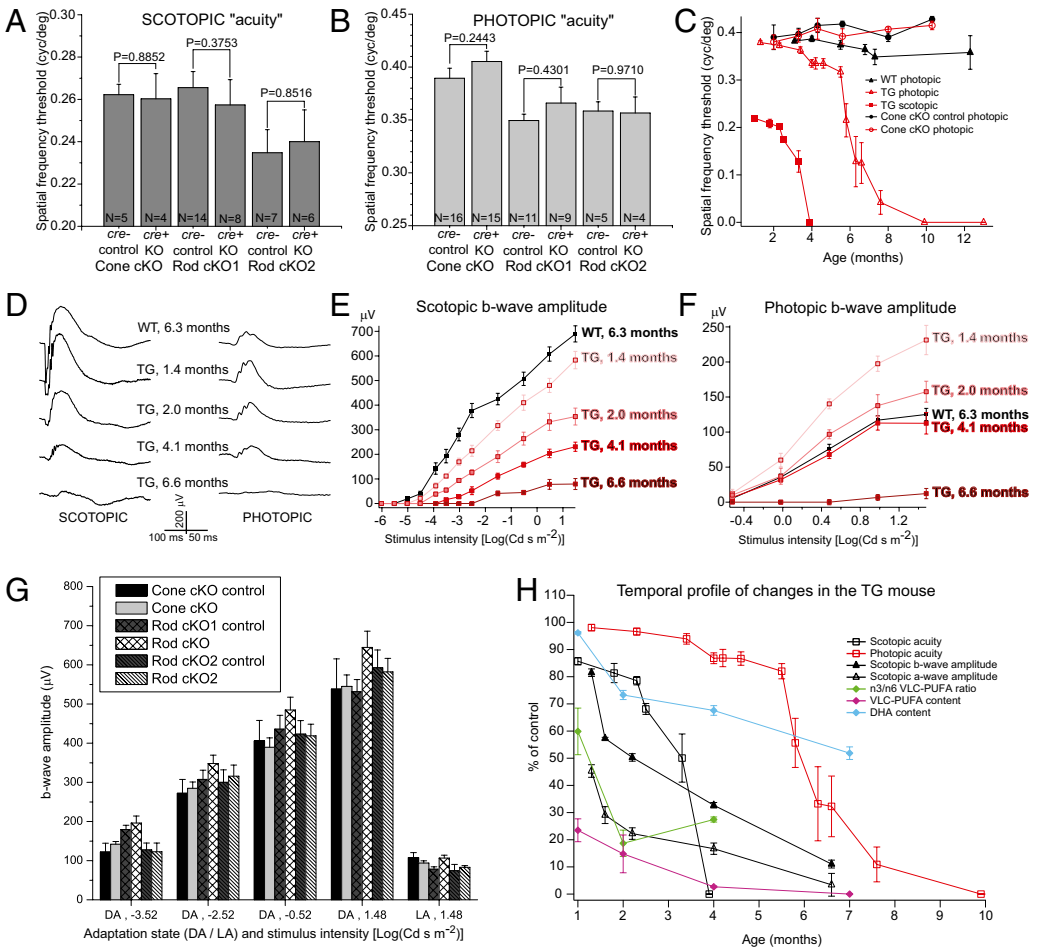

Fig. 4. (*A* and *B*) Visual acuity measured under scotopic (*A*) or photopic (*B*) conditions. cKO and congenic (*cre*$^-$) control mice show similar spatial visual thresholds of the optomotor reflex. (*C*) Visual performance in the cone cKO strain does not decrease up to 10 mo of age, whereas the TG strain shows a progressive decline compared with the TG control (WT) strain expressing the WT human *ELOVL4* allele. (*D*) Averages of raw scotopic ERG traces elicited by 1.48-log (cd·s·m^{-2}) flashes in TG mice show a progressive decline with the a-waves reduced already at 1.4 mo (n = 6), a decline exacerbated at 2.0 (n = 6), 4.1 (n = 3), and 6.6 (n = 3) mo. Photopic responses are unaffected or increased up to 6.6 mo. (*E* and *F*) Analysis of scotopic (*E*) and photopic (*F*) b-wave amplitudes in the TG strain reveal rod failure, followed by compromised cone function. (*G*) Rod and cone cKO strains do not show significant decreases in b-wave amplitudes under scotopic (DA) or photopic (LA) conditions. (*H*) Visual acuity, ERG a- and b-wave amplitudes, VLC-PUFA, DHA levels, and VLC-PUFA n3/n6 ratios are plotted as a function of time. The biochemical parameters are expressed as percentage of age-matched WT C57BL/6J mice. The physiological parameters (acuity and a- and b-waves) are normalized to data from 6.3-mo-old TG WT mice. All images show mean ± SEM.

VLC-PUFA content by ~58%. The *opsin–iCre75* driver (22) in our cKO2 strain was more efficient in excising *Elovl4* (~89% decrease in the mRNA) and reducing VLC-PUFA content (~98% decrease). Nonetheless, ERG and visual behavioral parameters in cKO2 mice were comparable with the parameters measured in congenic *cre*$^-$ controls, suggesting that residual ELOVL4 activity associated with columnar expression of *Elovl4*-positive photoreceptors in cKO1 rods is not required for the rescue of rod function. Because cone cKOs also displayed no electrophysiological or behavioral phenotype, we conclude that VLC-PUFA production is not required for photoreceptor survival and visual function in adult mice. It is still possible that cKO mice will exhibit functional deficits after >10 mo or that VLC-PUFAs can maintain function at very low (~2%) concentrations.

By pointing at the distinct etiologies conferred by the ablation of the mouse *Elovl4* gene vs. expression of human *ELOVL4*^{STGD3} in mouse photoreceptors, our data highlight the differences in the physiological impact of reducing retinal VLC-PUFA content in two different mouse models (KO vs. TG) of STGD3. In contrast to the human macular disease, which primarily affects cones, mouse retinas expressing the mutant human STGD3 allele showed massive rod degeneration. Deficits in cone signaling were detected only after rod function was mostly lost, suggesting the characteristic rod–cone dystrophic sequence. Thus, TG mouse strains expressing the human mutant protein might not represent appropriate models for human SGTD3 (37).

The mechanism underlying rod degeneration in ELOVL4^{STGD3} mice is currently unclear. Our data argue against a major role of ER stress and the UPR, because no significant differences in transcripts coding for the major UPR routes were detected. This finding is consistent with the recent analysis of Bip and XBP1 transcript/protein expression in another STGD3 mouse model (14). As suggested in heterologous expression studies, the TG phenotype might involve mislocalization and aggregation of the overexpressed mutant protein (11, 15, 18), with attendant pleiotropic effects of such aggregates (38). Indeed, formation of metabolically stable protein aggregates has been implicated in several neurodegenerative diseases (39).

In summary, we report that conditional ablation of *Elovl4* significantly reduces VLC-PUFA content but has no immediate deleterious effect on rod and cone survival or scotopic or photopic vision. Contrary to the knockouts, expression of the STGD3-causing mutant ELOVL4 protein induces early onset progressive rod–cone dystrophy in the mouse.

Methods

Mice. All procedures were approved by the Institutional Animal Care and Use Committee at the University of Utah, following the guidelines established by the Association for Research in Vision and Ophthalmology Statement for the Use of Animals in Ophthalmic and Vision Research. C57BL/6J and *rd1* (*PDE6b*^{rd1}) mice were from JAX. Cone and rod cell-specific KO mice were obtained from *Elovl4*$^{flox/flox}$ and *opsin–cre* mice (rod cKO1) (23), *opsin–iCre75* (rod cKO2) (25), or *HRGP*–cre mice (cone cKO) (24). TG control (WT) and experimental (TG) mice were generated by inserting the WT (*ELOVL4*^{WT}) or the STGD3 allele (*ELOVL4*^{STGD3}) of the human *ELOVL4* gene, respectively into the mouse genome with a cellular retinaldehyde-binding protein promoter (11).

Determination of Retinal Lipid Content. GC-MS analysis was optimized as described (9) by using a protocol that detects VLC-PUFA species from pairs of mouse retinas. Retinas were flash frozen in CO_2 and kept at –80 °C in argon. Samples and internal standards (50 µg of tridecanoic acid and 1.15 µg of

hentriacontanoic acid) were transferred to 2-mL stainless steel vials and homogenized with 0.7-mL beads and 1 mL of hexane–isopropanol (3:2). Homogenized samples were sonicated, and the extracts were dried with nitrogen. After methyl transesterification, samples were purified by solid phase extraction. LC- and VLC-PUFA content was determined by using GC-MS on an Rxi-5MS column.

Assessment of Visual Behavior and ERG. Optomotor reflex-based tests were conducted as described (32) by using the OptoMotry system (Cerebral Mechanics). Rotation speed (12 degrees/s) and contrast were kept constant. Cone-mediated vision was tested in mice adapted to room light (150–250 lx). Rod-dependent behavior was tested in dark-adapted mice by using LCD displays covered by ND16 neutral density filters (LEE Filters). The experimenter was blind to the genotype of the mice. ERG field potentials were measured as described (32) by using a UTAS BigShot Ganzfeld system (LKC Technologies). Scotopic and photopic ERGs were recorded by using increasing flash intensities using 3–11 mice of each group (cre^- control and cre^+ cKO). Two to 12 a- and b-wave traces were averaged for every stimulus intensity.

RT-PCR and Histology. Gene expression measurements of whole retinas were performed as described (32). Primer sequences are shown in *SI Text*. Amplified *Elovl4, Rho, Opn1mw, Opn1sw, GFAP, Perk, Ire1, Chop, Atf6*, and *Bip* mRNAs were referenced to *Gapdh* signals for each sample. Four to 12 independent samples (separate animals) were used in duplicates/triplicates and normalized to controls.

Immunohistochemical analysis of frozen vertical retinal sections was performed as described (32). Cryosections were permeabilized with 0.5% (vol/vol) Triton X-100, blocked with 10% (vol/vol) goat serum, and incubated with primary antibodies, cre (Covance; mouse, 1:500), *ELOVL4* (courtesy of Robert E. Anderson (University of Oklahoma, Oklahoma City, OK); rabbit, 1:150), and cone arrestin (courtesy of Wolfgang Baehr, University of Utah; rabbit, 1:500), overnight at 4 °C. Secondary antibodies were applied for 1 h at room temperature. Sections were examined by confocal microscopy.

Histological and electron microscopic analysis was performed as in ref. 40. Samples were dehydrated and embedded in epon, sectioned at 0.25 μm, deplasticized, and stained with toluidine blue for counting cell rows and measuring thickness of ONL (ImageJ; NIH). The average cell row number and thickness were determined for a 2.5-mm length of the retina in both directions from the optic nerve. Electron micrographs were prepared by using osmicated vertical slices, and multitile images were captured on a JEOL JEM-1400 transmission electron microscope.

Statistical Analysis. Data in this paper are presented as mean ± SEM. Two-tailed unpaired Student *t* test with Welch correction (unequal variations) was used to compare two groups of data, unless noted otherwise. Bonferroni correction was used for multiple statistical comparisons. Differences were considered statistically significant at $P < 0.05$.

ACKNOWLEDGMENTS. We thank Drs. Kang Zhang (University of California at San Diego) for providing floxed *Elovl4* and TG mice, Yun-Zheng Le (University of Oklahoma) for *HRGP–cre* and *opsin–cre* mice, Robert Anderson for the ELOVL4 antibody, Ryan Terry (University of Utah) for lipid extraction, W. Drew Ferrel (University of Utah) for help with plastic sections, and Wolfgang Baehr for the cone arrestin antibody. This work was supported by National Institutes of Health Grants EY13870, EY022076 (to D.K.), and EY014800 (to P.B., P.S.B., and D.K.); the Foundation Fighting Blindness (P.S.B. and D.K.); the Knights Templar Foundation (P.B.); the International Retina Research Foundation (P.B.); the Macula Vision Research Foundation (P.S.B.); the Thome Memorial Foundation (B.W.J.); Research to Prevent Blindness (B.W.J.); the Department of Defense (D.K.); and an unrestricted grant from Research to Prevent Blindness (to the Moran Eye Institute).

1. SanGiovanni JP, Chew EY (2005) The role of omega-3 long-chain polyunsaturated fatty acids in health and disease of the retina. *Prog Retin Eye Res* 24(1):87–138.
2. Guillou H, Zadravec D, Martin PG, Jacobsson A (2010) The key roles of elongases and desaturases in mammalian fatty acid metabolism: Insights from transgenic mice. *Prog Lipid Res* 49(2):186–199.
3. McMahon A, Kedzierski W (2010) Polyunsaturated very-long-chain C28-C36 fatty acids and retinal physiology. *Br J Ophthalmol* 94(9):1127–1132.
4. Agbaga MP, et al. (2008) Role of Stargardt-3 macular dystrophy protein (*ELOVL4*) in the biosynthesis of very long chain fatty acids. *Proc Natl Acad Sci USA* 105(35): 12843–12848.
5. Bernstein PS, et al. (2001) Diverse macular dystrophy phenotype caused by a novel complex mutation in the *ELOVL4* gene. *Invest Ophthalmol Vis Sci* 42(13):3331–3336.
6. Zhang K, et al. (2001) A 5-bp deletion in *ELOVL4* is associated with two related forms of autosomal dominant macular dystrophy. *Nat Genet* 27(1):89–93.
7. Molday RS, Zhang K (2010) Defective lipid transport and biosynthesis in recessive and dominant Stargardt macular degeneration. *Prog Lipid Res* 49(4):476–492.
8. Hubbard AF, Askew EW, Singh N, Leppert M, Bernstein PS (2006) Association of adipose and red blood cell lipids with severity of dominant Stargardt macular dystrophy (STGD3) secondary to an *ELOVL4* mutation. *Arch Ophthalmol* 124(2):257–263.
9. Liu A, Chang J, Lin Y, Shen Z, Bernstein PS (2010) Long-chain and very long-chain polyunsaturated fatty acids in ocular aging and age-related macular degeneration. *J Lipid Res* 51(11):3217–3229.
10. Agbaga MP, Mandal MN, Anderson RE (2010) Retinal very long-chain PUFAs: new insights from studies on *ELOVL4* protein. *J Lipid Res* 51(7):1624–1642.
11. Karan G, et al. (2005) Lipofuscin accumulation, abnormal electrophysiology, and photoreceptor degeneration in mutant *ELOVL4* transgenic mice: A model for macular degeneration. *Proc Natl Acad Sci USA* 102(11):4164–4169.
12. Kuny S, et al. (2010) Inner retina remodeling in a mouse model of stargardt-like macular dystrophy (STGD3). *Invest Ophthalmol Vis Sci* 51(4):2248–2262.
13. Dornstauder B, et al. (2012) Dietary docosahexaenoic acid supplementation prevents age-related functional losses and A2E accumulation in the retina. *Invest Ophthalmol Vis Sci* 53(4):2256–2265.
14. McMahon A, Jackson SN, Woods AS, Kedzierski W (2007) A Stargardt disease-3 mutation in the mouse *Elovl4* gene causes retinal deficiency of C32-C36 acyl phosphatidylcholines. *FEBS Lett* 581(28):5459–5463.
15. Ambasudhan R, et al. (2004) Atrophic macular degeneration mutations in *ELOVL4* result in the intracellular misrouting of the protein. *Genomics* 83(4):615–625.
16. Karan G, Yang Z, Zhang K (2004) Expression of wild type and mutant *ELOVL4* in cell culture: Subcellular localization and cell viability. *Mol Vis* 10:248–253.
17. Karan G, et al. (2005) Loss of ER retention and sequestration of the wild-type *ELOVL4* by Stargardt disease dominant negative mutants. *Mol Vis* 11:657–664.
18. Grayson C, Molday RS (2005) Dominant negative mechanism underlies autosomal dominant Stargardt-like macular dystrophy linked to mutations in *ELOVL4*. *J Biol Chem* 280(37):32521–32530.
19. Li W, et al. (2007) Depletion of ceramides with very long chain fatty acids causes defective skin permeability barrier function, and neonatal lethality in *ELOVL4* deficient mice. *Int J Biol Sci* 3(2):120–128.
20. McMahon A, et al. (2007) Retinal pathology and skin barrier defect in mice carrying a Stargardt disease-3 mutation in elongase of very long chain fatty acids-4. *Mol Vis* 13:258–272.
21. Vasireddy V, et al. (2007) Loss of functional ELOVL4 depletes very long-chain fatty acids (> or =C28) and the unique omega-O-acylceramides in skin leading to neonatal death. *Hum Mol Genet* 16(5):471–482.
22. Li S, et al. (2005) Rhodopsin-iCre transgenic mouse line for Cre-mediated rod-specific gene targeting. *Genesis* 41(2):73–80.
23. Le YZ, et al. (2006) Mouse opsin promoter-directed Cre recombinase expression in transgenic mice. *Mol Vis* 12:389–398.
24. Le YZ, et al. (2004) Targeted expression of Cre recombinase to cone photoreceptors in transgenic mice. *Mol Vis* 10:1011–1018.
25. Xu C, Bailly-Maitre B, Reed JC (2005) Endoplasmic reticulum stress: Cell life and death decisions. *J Clin Invest* 115(10):2656–2664.
26. Carter-Dawson LD, LaVail MM, Sidman RL (1978) Differential effect of the rd mutation on rods and cones in the mouse retina. *Invest Ophthalmol Vis Sci* 17(6):489–498.
27. Maekawa M, et al. (2010) Excessive ingestion of long-chain polyunsaturated fatty acids during developmental stage causes strain- and sex-dependent eye abnormalities in mice. *Biochem Biophys Res Commun* 402(2):431–437.
28. Penn RD, Hagins WA (1972) Kinetics of the photocurrent of retinal rods. *Biophys J* 12(8):1073–1094.
29. Robson JG, Frishman LJ (1995) Response linearity and kinetics of the cat retina: The bipolar cell component of the dark-adapted electroretinogram. *Vis Neurosci* 12(5): 837–850.
30. Prusky GT, Alam NM, Beekman S, Douglas RM (2004) Rapid quantification of adult and developing mouse spatial vision using a virtual optomotor system. *Invest Ophthalmol Vis Sci* 45(12):4611–4616.
31. Douglas RM, et al. (2005) Independent visual threshold measurements in the two eyes of freely moving rats and mice using a virtual-reality optokinetic system. *Vis Neurosci* 22(5):677–684.
32. Barabas P, et al. (2011) Missing optomotor head-turning reflex in the DBA/2J mouse. *Invest Ophthalmol Vis Sci* 52(9):6766–6773.
33. Rotstein NP, Aveldaño MI (1988) Synthesis of very long chain (up to 36 carbon) tetra, penta and hexaenoic fatty acids in retina. *Biochem J* 249(1):191–200.
34. Harkewicz R, et al. (2012) Essential role of ELOVL4 protein in very long chain fatty acid synthesis and retinal function. *J Biol Chem* 287(14):11469–11480.
35. Bazan NG, Gordon WC, Rodriguez de Turco EB (1992) Docosahexaenoic acid uptake and metabolism in photoreceptors: Retinal conservation by an efficient retinal pigment epithelial cell-mediated recycling process. *Adv Exp Med Biol* 318:295–306.
36. Carter-Dawson LD, LaVail MM (1979) Rods and cones in the mouse retina. I. Structural analysis using light and electron microscopy. *J Comp Neurol* 188(2):245–262.
37. Stone EM, et al. (1994) Clinical features of a Stargardt-like dominant progressive macular dystrophy with genetic linkage to chromosome 6q. *Arch Ophthalmol* 112(6):765–772.
38. Okuda A, et al. (2010) Hetero-oligomeric interactions of an *ELOVL4* mutant protein: implications in the molecular mechanism of Stargardt-3 macular dystrophy. *Mol Vis* 16:2438–2445.
39. Soti C, Csermely P (2002) Chaperones come of age. *Cell Stress Chaperones* 7(2):186–190.
40. Anderson JR, et al. (2009) A computational framework for ultrastructural mapping of neural circuitry. *PLoS Biol* 7(3):e1000074.